

AUTONOMOUS NAVIGATION ACCURACY USING SIMULATED
HORIZON SENSOR AND SUN SENSOR OBSERVATIONS

G. E. PEASE
and
H. T. HENDRICKSON

Summary

Infrared Earth horizon sensors in combination with a sun sensor have proven useful for autonomous station keeping of geosynchronous satellites but the complexity of a fully self-contained autonomous navigation system for low altitude satellites has discouraged implementation of such a scheme. A relatively simple system which would use horizon crossing indicators, a sun sensor, a quartz oscillator, and a microprogrammed computer is being studied.

The sensor combination is required only to effectively measure the angle between the centers of the Earth and the Sun. Simulations for a particular orbit indicate that 2 km r. m. s. orbit determination uncertainties may be expected from a system with 0.°06 measurement uncertainty. A key finding is that knowledge of the satellite orbit plane orientation can be maintained to this level because of the annual motion of the Sun and the predictable effects of Earth oblateness. The basic system described above can be updated periodically by transits of the Moon through the IR horizon crossing indicator fields of view. The extent to which these conclusions may be applied to a larger class of satellite orbits is under study.

Introduction

Previous autonomous navigation schemes (references 1 and 2) have had two characteristics which have caused them to be noncompetitive with normal ground navigation techniques; they tend to be low accuracy systems, yet they require inordinate onboard processing capability. Higher accuracy autonomous systems such as the Space Sextant are even more complex and require a large sacrifice of payload capability to perform the optical measurements and complex data reductions. To date, the most successful applications of the autonomous navigation concept have been for limited functions, most notably automatic longitude station keeping of geosynchronous satellites LES 6, LES 8, and LES 9 (references 3 and 4).

The present application of interest is for a self-contained low accuracy (12 k. m., 3σ) system with minimal payload allocation requirements. The success of this approach hinges less on accuracy than on degree of autonomy and simplicity. The trap we wish to avoid is the common one of proposing a massive and complex system that is able to overcome all possible problems other than those of cost, practicality, and self-sufficiency.

As envisioned, the completely self-contained on board navigation system will use one or more IR Earth horizon crossing indicators, a Sun sensor, a quartz oscillator, and a microprogrammed computer to deliver the desired overall orbit position accuracy of 12 k. m., 3σ , or better throughout a six month lifetime mission. Such a system has the potential to provide this level of self-contained autonomous navigation accuracy over very long mission lifetimes measured in years instead of months. It is important to keep in mind that the proposed system is truly autonomous in the sense that it is independent of other systems such as ground or orbiting radio beacons which are susceptible to jamming or destruction.

To date, a 470 km circular orbit with 34° inclination has been studied using a special version of the FLEXSAT program. A brief description of this program is given in Appendix B.

Sensor Measurement System

Figure 1 illustrates a conventional attitude sensor configuration that is well suited to perform autonomous navigation functions. The spinning satellite uses one or more narrow angle IR horizon crossing indicators and a wide angle Sun sensor. For autonomous navigation with horizon crossing indicators it is desirable to orient the spacecraft spin axis normal to the orbit plane as shown. This may be controlled by monitoring attitude throughout the orbital period and minimizing variations in the horizon scanner pulse widths by means of attitude maneuvers when required. The attitude measurements allow determination of the direction to the center of the Earth with respect to the Sun at each scan. As indicated, the horizon sensors can also detect the Moon. This opportunity will occur at least twice in a sidereal month. The moon observations provide an inertial reference update that normally would require the extra complexity of a separate star sensor system. For the system shown in figure 1, a wide angle sun sensor is used to measure the times of Sun crossings through the instrument field of view and the elevation of the sun with respect to the optical axis of the sun sensor. The horizon and Sun transit times, along with the Sun elevation, yield the angle between the centers of Earth and Sun as seen from the satellite.

An ambiguity exists in this measurement system, in that a rotation of the satellite orbit plane about the Earth-Sun line would be undetectable in the observations if the gravitational potential field of the Earth were that of a sphere rather than that of an oblate spheroid, and if the direction of the Sun in inertial space were fixed. The proposed system takes advantage of the known nature of Earth oblateness effects (see Appendix A) and of the orbital motion of Earth in the plane of the ecliptic. The dynamical effects of oblateness include regression of the nodes along the equator; the orbital motion of Earth defines the ecliptic plane. Periodic Moon observations remove any remaining ambiguity. Initial orbit knowledge at time of orbit injection should be sufficiently accurate (528 meters, 0.61 m/sec) to provide confidence that the ambiguity will not be a problem in practice.

Error Model

For the initial studies, the sensor measurements have been simulated in the form of angular distance between the centers of Earth and Sun at one minute intervals during the portion of the orbit in which the Sun is visible to the satellite. An uncertainty of 1700 m (reference 5) was assumed for the uncertainty in the height of the 14-16 micron absorption layer of Earth's atmosphere. This translates to a horizon sensor angular measurement error of

$$\sigma_{\theta_h} = 0.042$$

for a 470 km altitude orbit.

The Sun sensor can measure angular position of the Sun to

$$\sigma_{\theta_s} = 0.03$$

and the angular uncertainty between the optical axes of the horizon and Sun sensors is

$$\sigma_{\theta_a} = 0.02.$$

We consider time-tag uncertainties resulting from instrumental delay and clock error to be similar in magnitude to σ_{θ_a} . The uncertainty, σ_{θ} in the angle between the center of Earth and center of Sun is approximately the r. s. s. of these errors or

$$\sigma_{\theta} = (\sigma_{\theta_h}^2 + \sigma_{\theta_s}^2 + 2 \sigma_{\theta_a}^2)^{1/2} \approx 0.06,$$

which is the angular uncertainty used in the simulations.

FLEXSAT was used to generate state vector covariance matrices based on the angular measurement uncertainties. The ballistic drag value, $C_D A/W$, was also estimated. In addition, the Kalman filter performance was tested by perturbing the initial values of the estimated parameters

by the amount of the a priori uncertainties. These uncertainties are listed in Table 1. The reference trajectory value of $C_D A/W$ was $0.037 \text{ m}^2/\text{kg}$.

Additional filter errors were introduced by modelling an eighth degree, eighth order geopotential field in the numerical integration of the reference trajectory used to generate the simulated observations, whereas a second degree, zero order fit model was used. Corresponding covariance uncertainties were roughly approximated by adding process noise to the covariances in the form of acceleration uncertainties,

$$\sigma \dot{x}, \dot{y}, \dot{z} = 80.2 \mu\text{g},$$

to represent high frequency geopotential accelerations and unmodeled aerodynamic drag variations. The low frequency J_2 term, in contrast, produces accelerations of up to about $1000 \mu\text{g}$. The simple analytic disturbing function of Appendix A serves to model the J_2 accelerations very precisely. The velocity vector of a satellite in an inclined orbit is therefore surprisingly determinable in equatorial coordinates without a stellar reference.

Effect of Orbit/Sun Geometry

Figure 2 illustrates the various possible extremes of geometry for a 34° inclination orbit, depending upon the time of day of launch and the time of year. Consider the Sun 1, Sun 2 and N axes to be in the plane of the drawing. The Sun 3 axis, equatorial plane, and satellite orbit plane are normal to the plane of the drawing. As shown, the Sun can be within $\pm 23.5^\circ$ of the equator, depending upon the time of year. Sun 1 and Sun 2 positions are extremes of solar declination. In the drawing they are placed normal to the satellite line of nodes so that at Sun 2 the maximum angle of the orbit plane to the sun line of 57.5° is attained. That this is unfavorable geometry is evident. At the limit, 90° is singular, for if the satellite attempted

to navigate by observing a celestial object at N, normal to the orbit plane, it is seen that in a circular orbit the Earth-object angle would not change as a function of time, to first order.

The Sun 3 geometry is also unfavorable, as the sunline is coplanar with the satellite orbit. Since this particular configuration again places the satellite line of nodes on the ecliptic line of nodes, the orbital inclination of the satellite is not directly observable.

Position Uncertainties

Table 2 contains the peak remaining radial, intrack, and crosstrack position standard deviations for each of the three extreme Sun orientations after nine simulated orbital revolutions of the satellite, using FLEXSAT covariances. An advantage of a recursive real time filter is that the customary prediction errors are limited to data gaps, which in this case are somewhat less than half of each orbit revolution.

The largest crosstrack errors are associated with Sun 1 orientation, with Sun 3 a close contender. Figures 3 and 4 plot the time history of these covariance-derived uncertainties as a function of time from injection. It is seen that the orbit solutions are stable but not overly convergent. Simulations with a spherical Earth model produce crosstrack uncertainties that increase with time, as expected, in the presence of the $80\mu\text{g}$ acceleration noise that simulates unmodeled high frequency geopotential and drag terms. This results from the ambiguity in the orientation of the orbit plane that would exist except for the measurable presence of the J_2 disturbing function.

The largest position uncertainty was found to be the intrack standard deviation in the Sun 2 configuration, which also produces the largest radial uncertainty (see Table 2). The time history from injection of these errors is plotted in figures 5 and 6. As expected, these exhibit more convergent behavior than do the crosstrack uncertainties, which more closely reflect orbit plane orientation errors. However, it should be noted that the highest intrack errors are initially large and do not converge to the extent of recovering a priori knowledge. The Earth horizon measurement errors, of course, map directly into intrack orbit errors.

Effect of Injection Knowledge

The previously described cases used the somewhat conservative orbit injection knowledge uncertainties and errors in Table 1 of

$$\sigma_{x,y,z} = \Delta_{x,y,z} = 3048 \text{ m}$$

$$\sigma_{\dot{x},\dot{y},\dot{z}} = \Delta_{\dot{x},\dot{y},\dot{z}} = 3.048 \text{ m/sec.}$$

The crosstrack errors for a typical nominal case (Sun at first point of Aries, $\Omega_{\text{Sat}} = 90^\circ$) are plotted from injection through nine orbit revolutions in Figure 7.

To verify the dependence of orbit plane orientation knowledge on injection knowledge and to test the capability of retaining this knowledge, a similar case with more realistic injection knowledge and errors was run using

$$\tilde{\sigma}_{x,y,z} = \tilde{\Delta}_{x,y,z} = 528 \text{ m}$$

$$\tilde{\sigma}_{\dot{x},\dot{y},\dot{z}} = \tilde{\Delta}_{\dot{x},\dot{y},\dot{z}} = 0.61 \text{ m/sec.}$$

Radial uncertainty was reduced from about 600 m (nominal case) to 400 m on the ninth orbit revolution, while intrack uncertainty was reduced from 2700m (nominal case) to 1900m on the ninth revolution. The important crosstrack uncertainty is plotted in Figure 8. It is seen that the injection knowledge of 528 m is retained through the ninth orbit revolution and even improved slightly between the first and ninth revolutions. This is certainly encouraging in light of the importance of minimizing orbit plane orientation errors. As expected, however, the solution displays slightly divergent characteristics. In time the errors might be expected to grow to the size of those in Figure 7.

Filter Errors

The largest filter estimate difference from the "truth" state vector or from the "truth" ballistic drag value is less than 3σ , where the value of σ is obtained from the covariance matrix associated with the particular

estimate. Assuming a Gaussian error distribution, one would normally expect to see an occasional 3σ estimate. The great majority of estimates are less than 1σ from the "truth" model. The actual estimates are accordingly better than Table 2 and Figures 3 - 8 indicate. In these cases the conservative process noise of $80.2\mu g$ served to maintain the filter covariance matrix at a reasonably high level. The fact that there was convergence and that the actual errors showed reasonable conformity with the sigmas from the covariance analysis indicates that the filter covariances are realistic. Since in theory they represent an infinite sample of Monte Carlo trials they are the numbers tabulated and plotted in this paper.

Moon Observations

Figure 1 illustrates how the horizon crossing indicator will, in general, view two portions of the Moon's orbit (the second view area is on the opposite sides of the satellite and Moon orbits). When the Moon enters these view areas, once every sidereal month for each portion, the 14-16 micron bandwidth horizon sensor will detect the Moon for several satellite orbit revolutions on each occasion. The exact length of viewing time depends upon the horizon sensor field of view and the inclination of the satellite orbit plane to the orbit plane of the Moon.

The Moon observations can be used to periodically update the orbit knowledge with independent observations. These observations fix the satellite state in inertial space in a direct manner. If two horizon crossing indicators are used in order to scan both north and south of the orbit plane, then two additional Moon viewing periods are available in each sidereal month. This system would seem to be superior to a system using only one horizon crossing indicator in any event, when the attitude determination problem is examined.

The principal value of Moon observations is to provide periodic recovery capability in the event that orbit knowledge is lost or degraded owing to larger than expected injection errors, degraded sun sensor performance, transient data stream/clock/microprocessor failures or unexpectedly large perturbations to the satellite orbit. A very compact,

pre-calculated lunar ephemeris would suffice because of the infrequency of Moon observations. With two horizon sensors, the Moon would nominally be observable for four or five orbit revolutions per week. To account for the large IR radiation differences between the illuminated hemisphere of the Moon and the dark side, a lunar phase-dependent model of the asymmetric sensor response would be a necessary part of the pre-calculated ephemeris. Figure 9 shows the essential elements of the navigation system, including the Moon data capability. The dashed lines indicate that the Sun elevation measurements are optional for attitude control, but may prove useful.

Clock Errors

All horizon, Sun, and Moon observations must be time-tagged by the onboard oscillator. A typical quartz oscillator is stable to one part in 10^9 , or 30 msec/year. To make use of 500 m injection accuracy we desire clock errors no larger than

$$\Delta t \leq \frac{500 \times 5640}{6848252 \times 2\pi} \approx 66 \text{ msec}$$

during the intervals between Moon observations, which is clearly not a problem. In the above example the orbital period is 5640 seconds and the orbit semimajor axis is 6848252 m.

Onboard Computer Requirements

The products of the autonomous system diagrammed in Figure 9 are the satellite ephemeris at bottom center and the attitude control function at upper right of the chart. The recursive orbit filter and attitude computations, ephemeris evaluation, and information management throughout the system could be performed by a microprogrammed I/O and central processor system. The requirements are currently being studied, but it is estimated that a 32k word memory and 16 bit fixed word length should be adequate.

Conclusions

An autonomous navigation system such as the one diagrammed in Figure 9 would appear to be capable of delivering accuracies normally associated with horizon sensors in conjunction with a stellar attitude system (reference 7). It is felt that the extra complication of a star sensor may be unwarranted considering the relatively good performance of a horizon sensor and sun sensor system. To fully assess the value of such a system, however, it is important to study the particular orbital characteristics of the intended mission. For example, simulations indicate that some high inclination missions may be a poor choice or would at least require further study. Accuracy will also be dependent to some extent on orbit altitude.

References:

1. "Autonomous Navigation Systems Technology Assessment," J. W. Lowrie, Martin Marietta Aerospace, AIAA Report No. 79-0056, January 1979.
2. "High Altitude Reference System Development Study," N. Westheimer, P. Andrews, J. Samson, Rockwell International Technical Report AFAL-TR-79-1111, Volume II, August 1979.
3. "Automatic Stationkeeping," A. Braga-Illa, J. Spacecraft, Vol. 6, No. 4, April 1979.
4. "Navigation Schemes for LES-8/9 Autonomous Stationkeeping System," S. Srivastava, MIT, Lincoln Laboratory Technical Note 1973-18, 20 April 1973.
5. "Located Horizon Variation Study," L. Bradfield, G. Nelson, Honeywell Inc. Report, NASA CR-6678, N69-36001, January, 1969.
6. "Digital Hardware for Use in Spacecraft Control Applications," G. Gilley, AAS 80-031, February, 1980.
7. "Analysis of an Horizon Scanner Autonomous Orbital Navigation System," J. S. Meditch, J. L. LeMay, J. P. Janus, Aerospace Corp., Report No. TDR-469(5540-10)-6, July 1965.

Appendix A

The disturbing function of an equatorial bulge is

$$D = -\frac{\mu}{2r^3} J_2 (3 \sin^2 \delta - 1)$$

where

μ is GM_{Earth} ,

r is the instantaneous radius vector,

J_2 is the second degree Legendre polynomial coefficient for Earth,

δ is the instantaneous declination of the satellite.

The secular perturbations are then

$$D_s = \frac{1}{2\pi} \int_0^{2\pi} D \, dM$$

where M is the mean anomaly.

In terms of orbital elements a , e , i , ω , Ω , M_0 , the principal secular effect is a regression of the nodes along the equator,

$$d\Omega_s = -\frac{3n J_2}{2a^2(1-e^2)^2} \cos i \, dt,$$

where n is the mean motion.

Depending upon whether orbital inclination is less than or greater than $i = \arcsin(2/\sqrt{5}) = 63.43^\circ$, the line of apsides will secularly advance or regress according to

$$d\omega_s = \frac{3n J_2}{2a^2(1-e^2)^2} \left(\frac{5}{2} \sin^2 i - 2 \right) dt.$$

Secular changes in the orbital period are also a function of a , e , and i as the mean anomaly changes by

$$dM_s = n \, dt \left[1 - \frac{3 J_2}{2a^2(1-e^2)^{3/2}} \left(\frac{3}{2} \sin^2 i - 1 \right) \right].$$

APPENDIX B

SIMULATION SOFTWARE

- program: FLEXSAT
- author: H. Hendrickson
- compiles on: CDC 7600, CDC 176 FORTRAN compiler
- trajectory: Runge-Kutta fourth order integrator
- filter: Kalman
- partial derivatives: finite difference

$$\Delta\theta = f(p_1, \dots, p_j + \Delta p_j, \dots, p_k)(t_j) - f(p_1, \dots, p_k)(t_j)$$

at the i th observation, θ_i and j th estimated parameter, p_j at time t_i for the data equation

$$\theta = f(p_1, \dots, p_k) + \epsilon$$

having k parameters, ϵ observation noise.

- Additive parameter noise model:
White acceleration noise,

$$\sigma_{\frac{q}{r}} = \sigma_{\frac{q}{r}} / (t_{i+1} - t_i)^{1/2}$$

APPENDIX C

ONBOARD CALCULATIONS FOR HORIZON/SUN SENSOR AUTONOMOUS ATTITUDE AND NAVIGATION SYSTEM

- Polynomial evaluation, one second intervals for observation angles,

3 Annual Terms

$$\theta_t(a, e, M_0)_{\text{Earth}}$$

8 Monthly Terms

(use different $\Delta \Omega$,
 $\Delta \omega$ each month)

$$\theta_t(a, e, i, \Omega, \omega, M_0, \Delta \Omega, \Delta \omega)_{\text{Moon}}$$

3 Secular terms
(Satellite orbit)

$$\theta_t(\Delta \Omega, \Delta \omega, \Delta M)_{J_{2,0} J_{2,2}}$$

- Sequential filter recursive estimation at each observation time

2 attitude angles (α , δ spin axis)

5 satellite orbit parameters

(a, e, i, Ω , ω , $C_D A/W$)
Satellite

and ballistic drag

(assume M_0 known at injection)

- Satellite ephemeris calculation

geocentric position

as a function of time (x, y, z)
at one minute intervals t

Table 1.

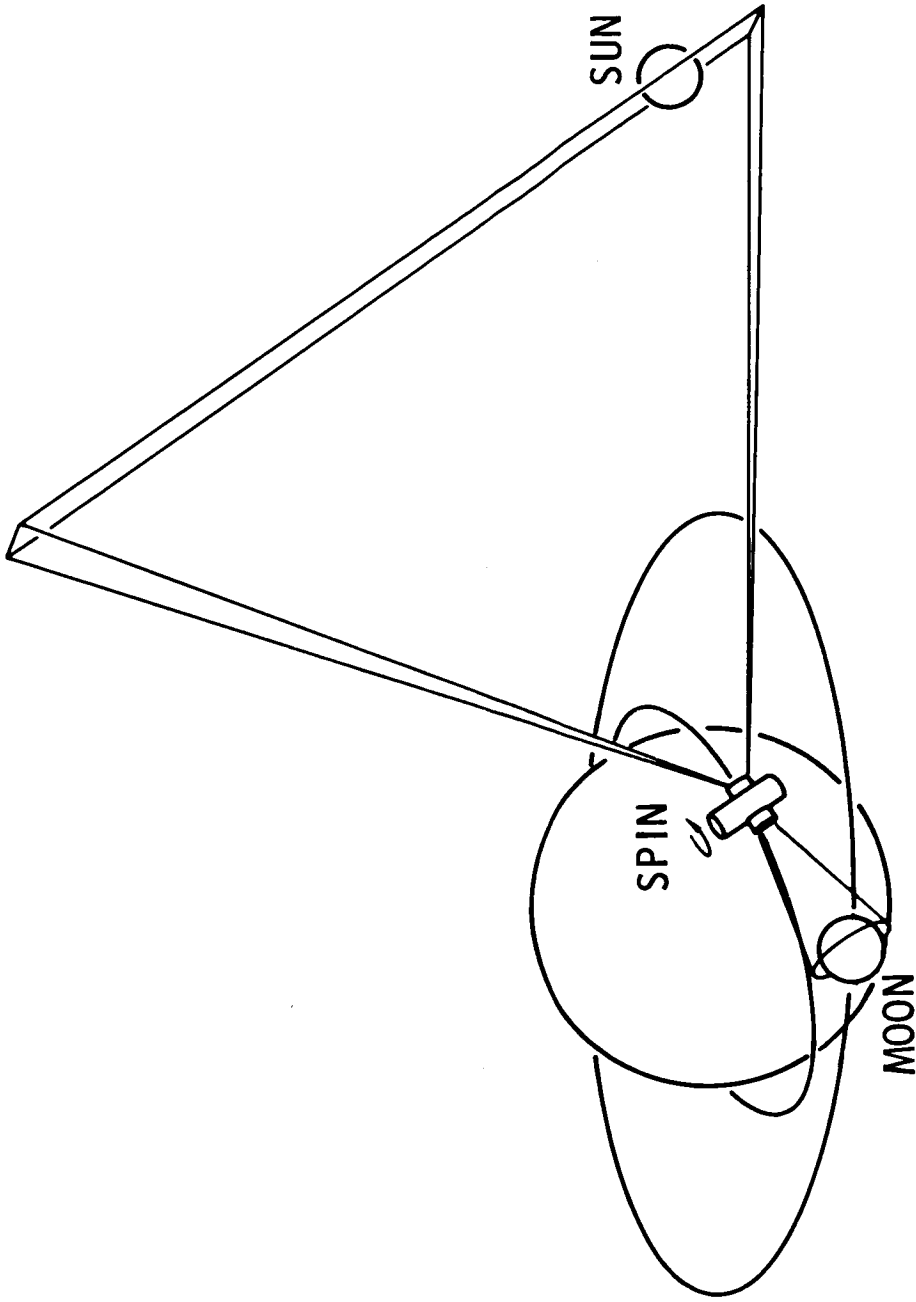
Simulation a priori Uncertainties/Initial Perturbations

<u>parameter, p</u>	$\tilde{\sigma}_p = \Delta p$ (initial)
x, y, z	3048 meters
$\dot{x}, \dot{y}, \dot{z}$	3.048 m/sec
$C_{D A/W}$	$8.19 \times 10^{-3} \text{ m}^2/\text{kg}$

Table 2.

EFFECTS OF EXTREME SUN VIEW GEOMETRY				
	9th REV	SUN 1 (10° .5)	SUN 2 (57° .5)	SUN 3 (COPLANAR)
σ	RADIAL (M)	490	730	430
σ	INTRACK (M)	1860	3440	1830
σ	CROSSTRACK (M)	2960	1620	2740
σ	r.m.s. (M)	2040	2230	1920

Figure 1



**SCHEMATIC OF PROPOSED HORIZON CROSSING INDICATOR AND WIDE ANGLE SUN SENSOR
CONFIGURATION ON A SPINNING SATELLITE WITH SPIN AXIS NORMAL
TO THE SATELLITE ORBIT PLANE**



Figure 2

Extremes of Possible Sun View Geometry

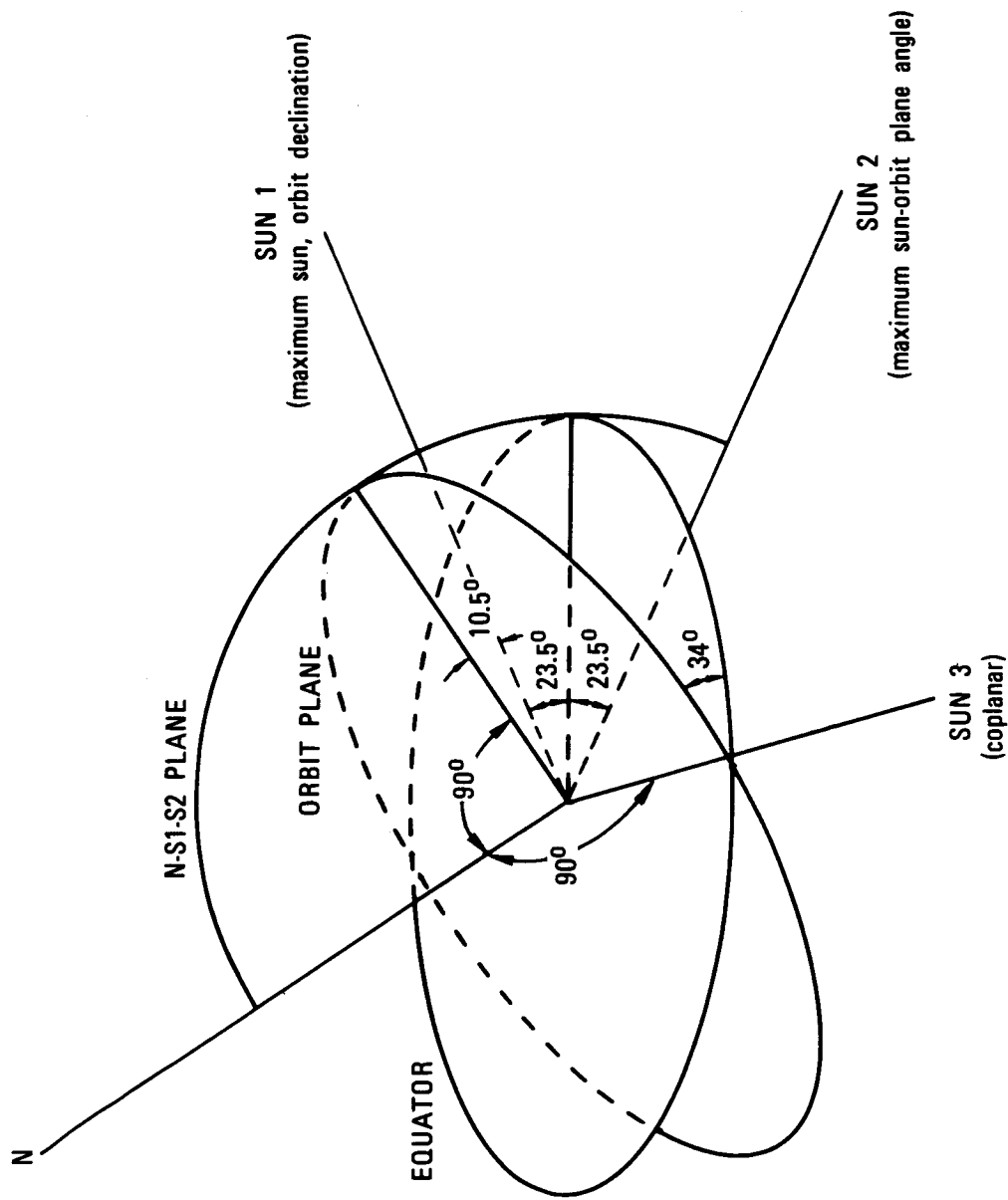


Figure 3

Crosstrack Error, Worst Case SUN 1

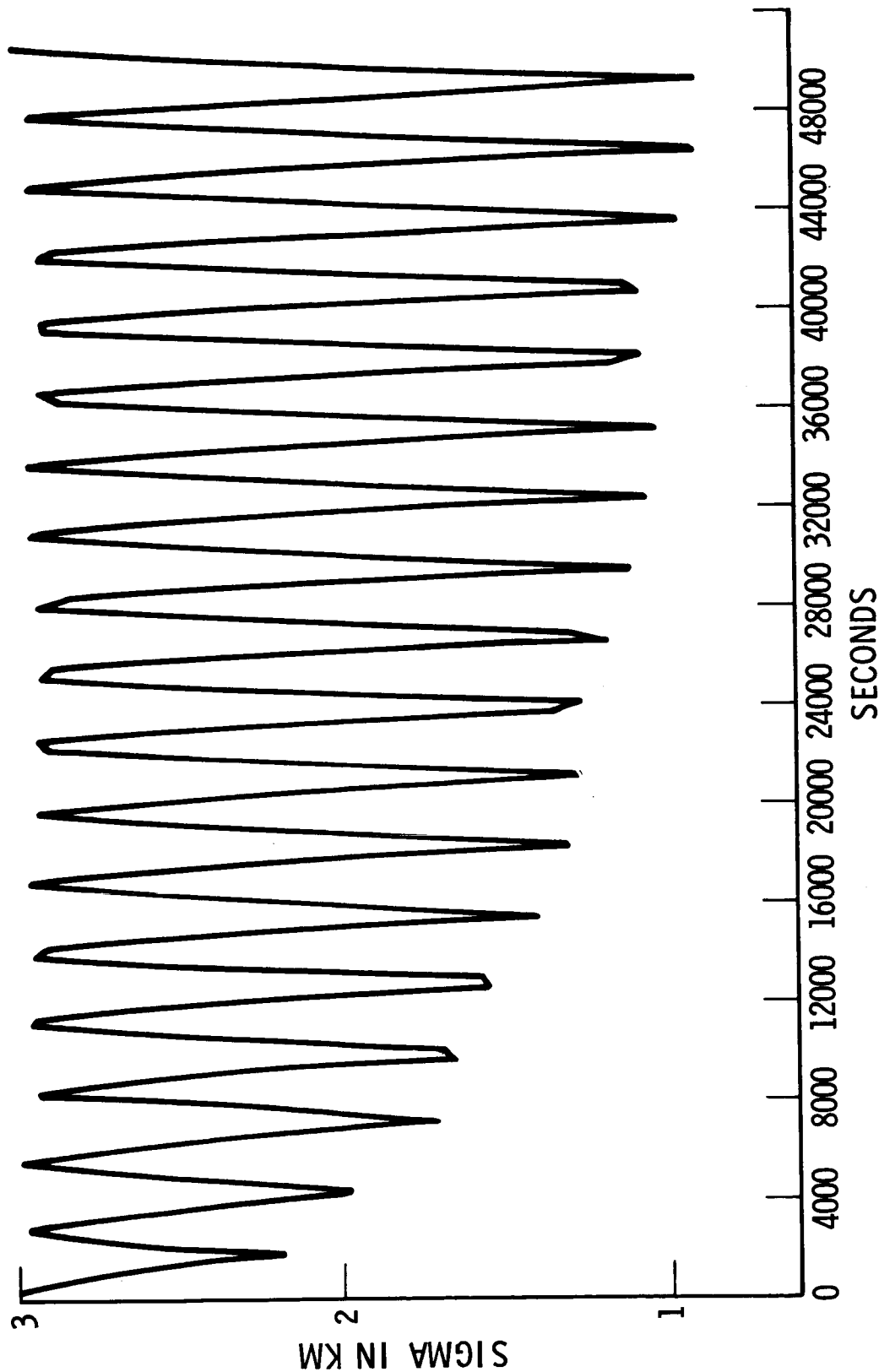
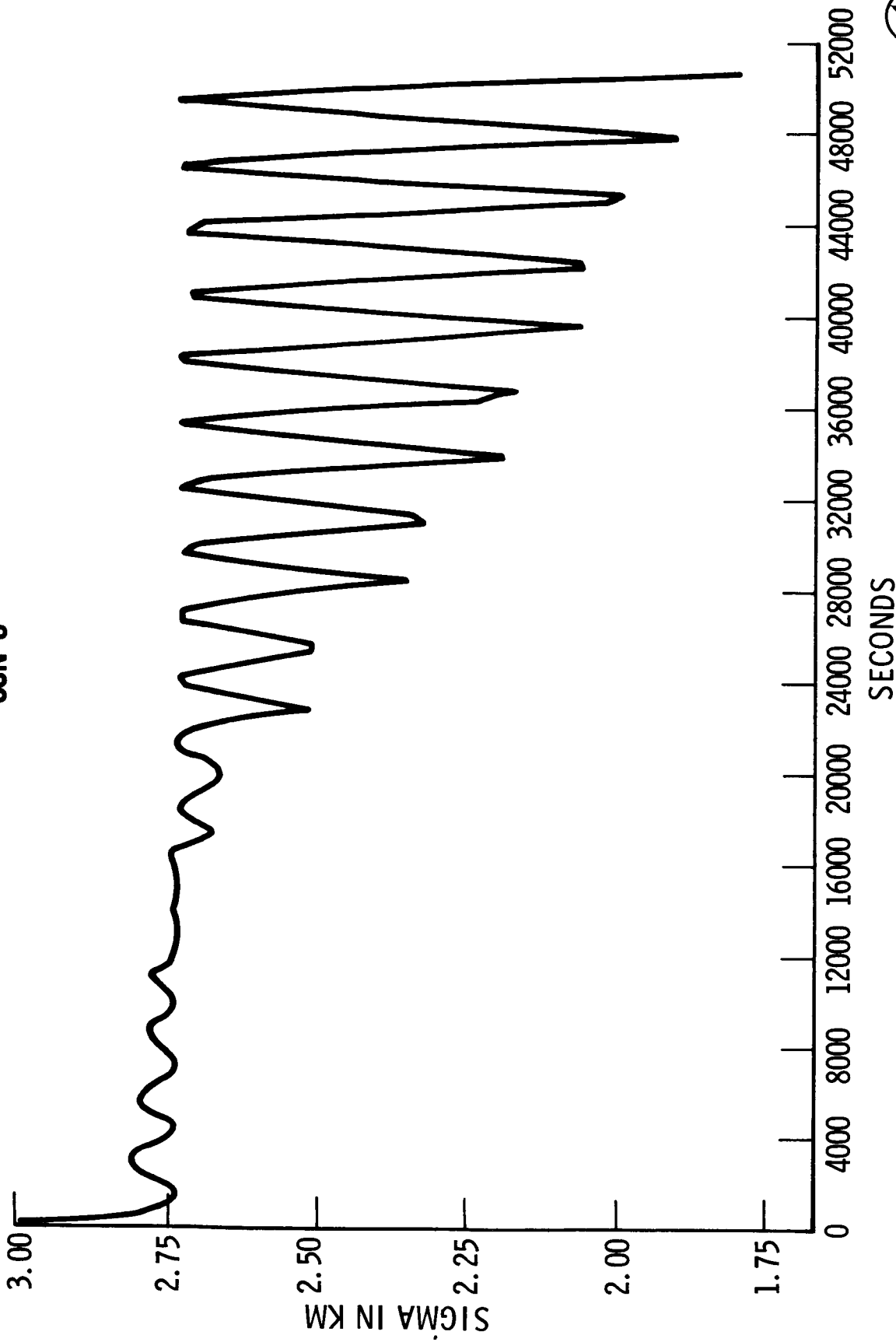


Figure 4

Crosstrack Error, Sun on Line of Nodes SUN 3



+

+

Figure 5

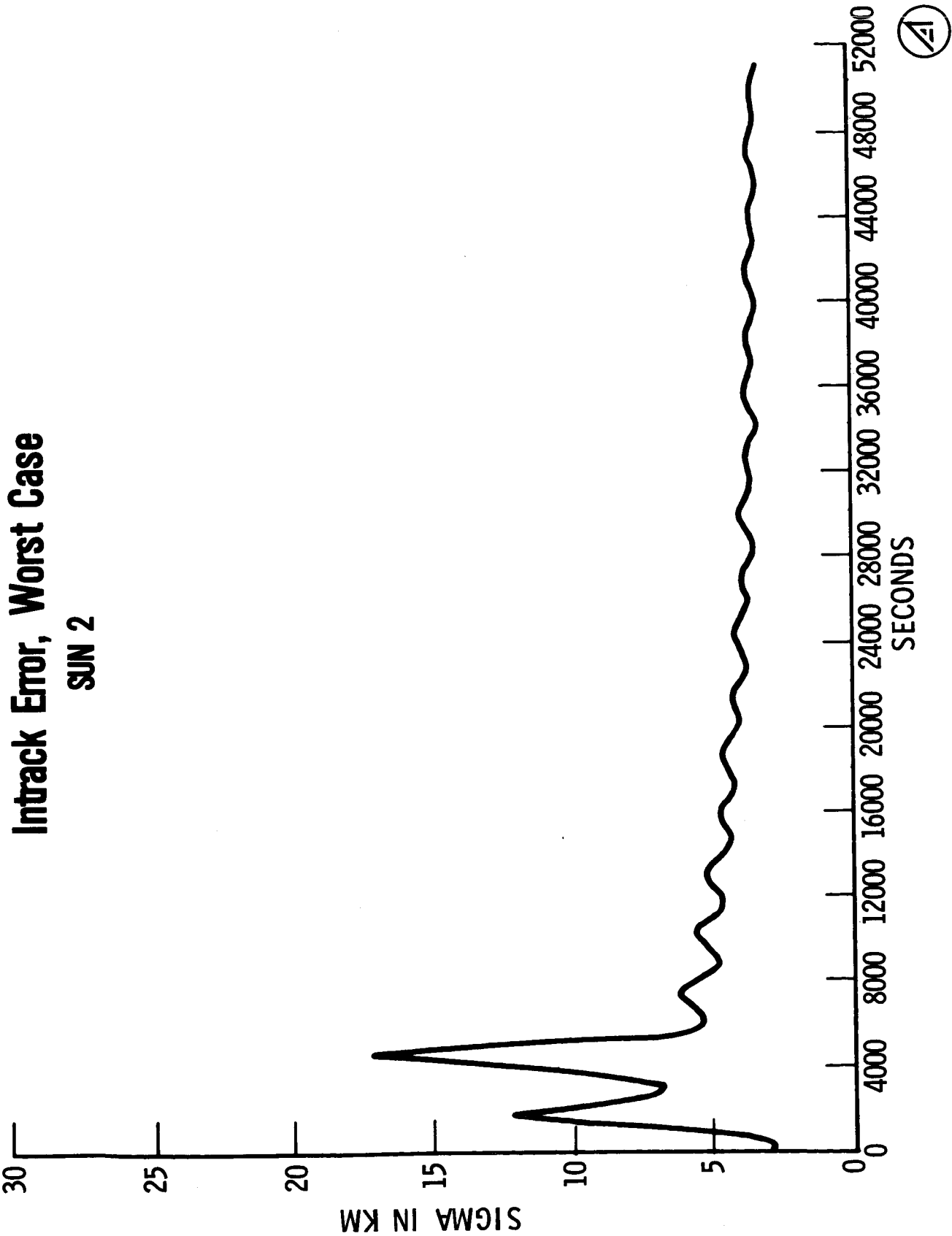


Figure 6

Radial Error, Worst Case

SUN 2

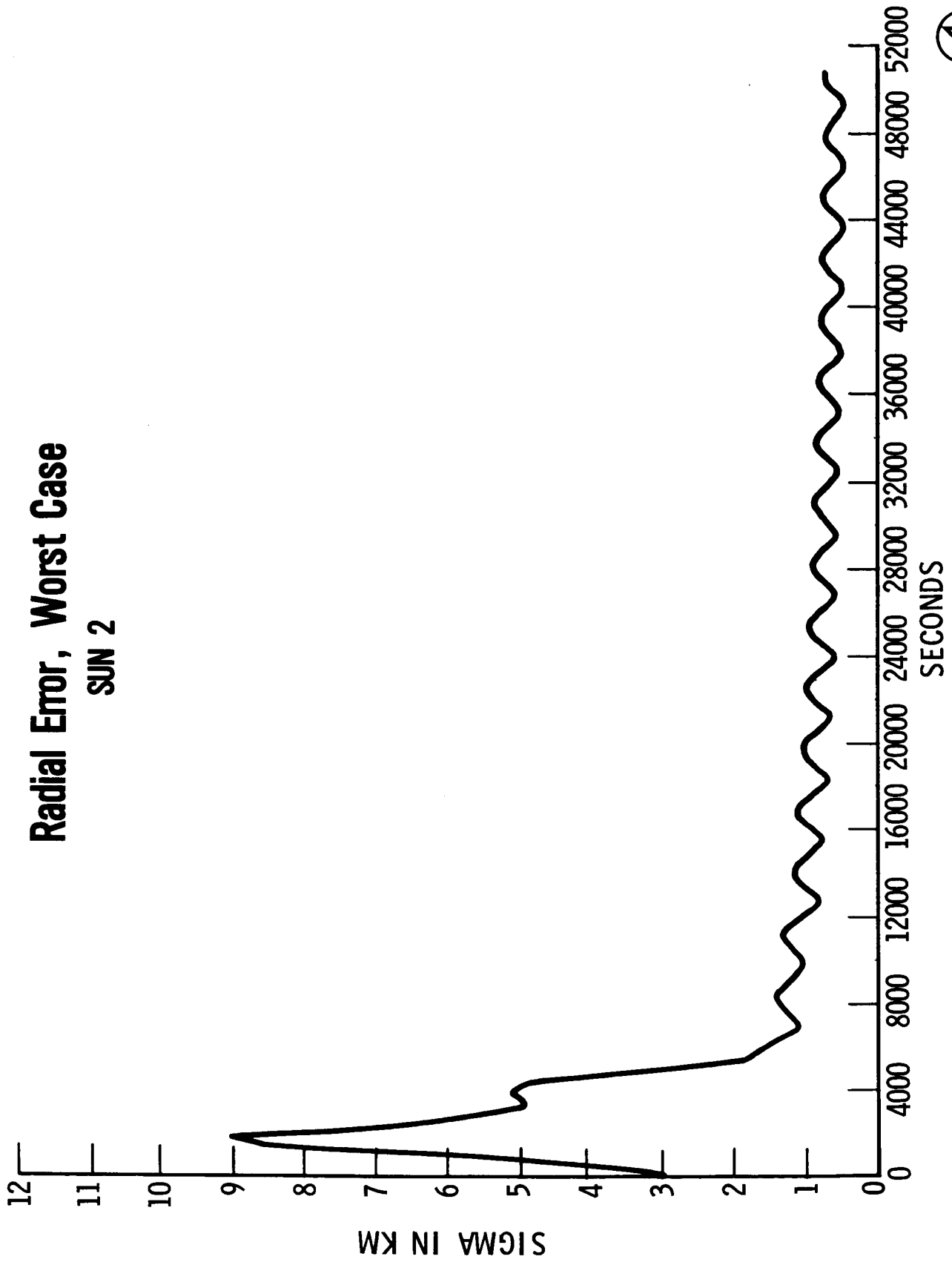
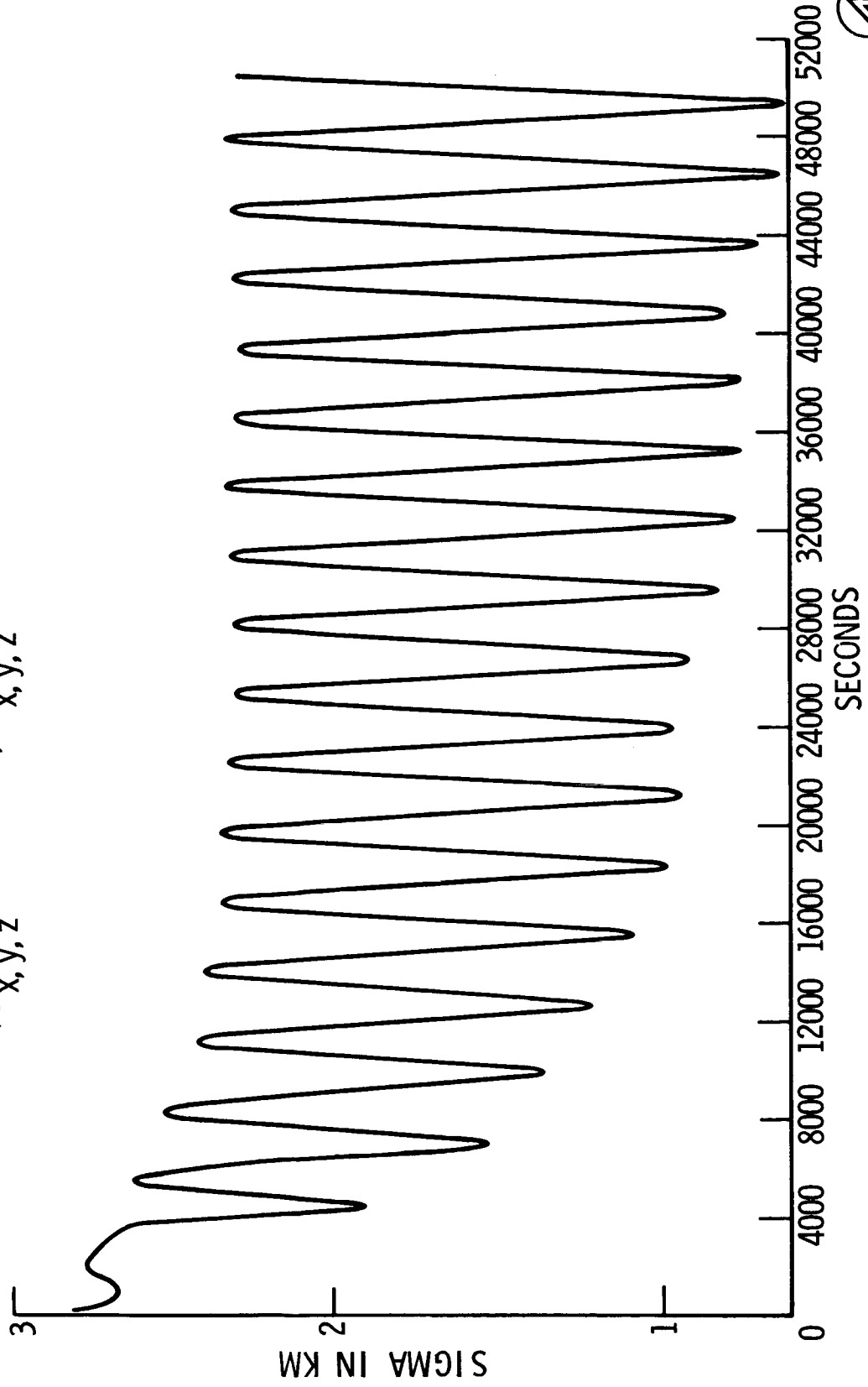


Figure 7

Crosstrack Error

NOMINAL A PRIORI CASE

$$(\tilde{\sigma}_{x,y,z} = 3.05 \text{ KM}, \dot{\tilde{\sigma}}_{x,y,z} = 3.05 \text{ M/sec})$$



+

+

Crosstrack Error

IMPROVED A PRIORI CASE

$(\tilde{\sigma}_{x,y,z} = 528 \text{ METERS}, \dot{\tilde{\sigma}}_{x,y,z} = 0.61 \text{ M/sec}$

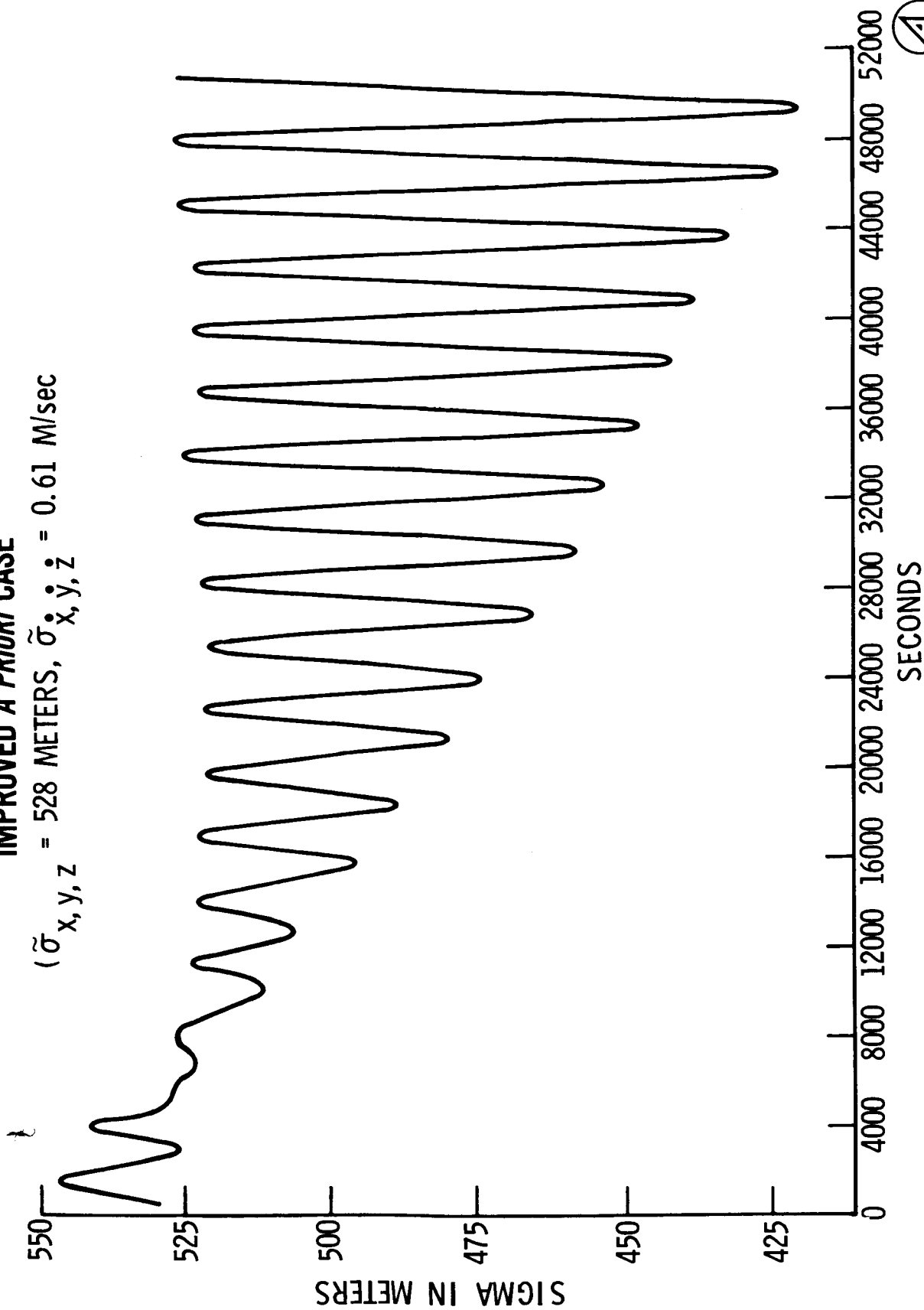


Figure 8

+

+

Figure 9

Horizon Indicator/Sun Sensor AUTONOMOUS NAVIGATION SYSTEM FOR SPINNING SATELLITE

